Supporting Information
for
Predicting a Generalized Mechanism of Branched Hydrogenolysis on Ru, Ir, and Pt Surfaces for Polymer Upcycling Applications

Andy Simonson,[1] Lydia Thies,[1] and David Hibbitts[1,2]*
[1]*Department of Chemical Engineering, University of Florida, Gainesville, FL 32611*
[2]*Davidson School of Chemical Engineering, Purdue University, West Lafayette, IN 47907*

*Corresponding author: hibbitts@purdue.edu

Table of Contents

1. Temperature Corrected Enthalpies, Entropies, and Gibbs Free Energies

Enthalpies (H) and Gibbs free energies (G) can be calculated from density functional theory (DFT)-derived energies using statistical mechanics as described in the methods section. (Eq. 4-5)

Adsorbed species are not considered to have translational or rotational contributions; all such motions are modeled as frustrated vibrations on the metal surface. Vibrational, rotational, and translational enthalpies and free energies are estimated from other statistical mechanics formalisms:

$$ZPVE = \sum_i \left(\frac{1}{2} h\nu_i\right) \tag{S1}$$

$$H_{vib} = \sum_i \left(\frac{h\nu_i \exp\left(-\frac{h\nu_i}{kT}\right)}{1-\exp\left(-\frac{h\nu_i}{kT}\right)}\right) \tag{S2}$$

$$G_{vib} = \sum_i \left(-kT\ln\left(\frac{1}{1-\exp\left(-\frac{h\nu_i}{kT}\right)}\right)\right) \tag{S3}$$

$$H_{trans} = \frac{5}{2} kT \tag{S4}$$

$$H_{rot,linear} = kT \tag{S5}$$

$$H_{rot,nonlinear} = \frac{3}{2} kT \tag{S6}$$

$$G_{trans} = -kT\ln\left(\left(\frac{2\pi mkT}{h^2}\right)^{\frac{3}{2}} V\right) \tag{S7}$$

$$G_{trans} = -kT\ln\left(\frac{\pi^{\frac{1}{2}}}{\sigma}\left(\frac{T^3}{\theta_x\theta_y\theta_z}\right)^{\frac{1}{2}}\right) \tag{S8}$$

$$\theta_i = \frac{h^2}{8\pi^2 I_i k} \tag{S9}$$

Where I_i is the moment of inertia about the i axis (either x, y, or z) and σ is the symmetry number of the species.[1]

2. Activation enthalpies, entropies, and free energies

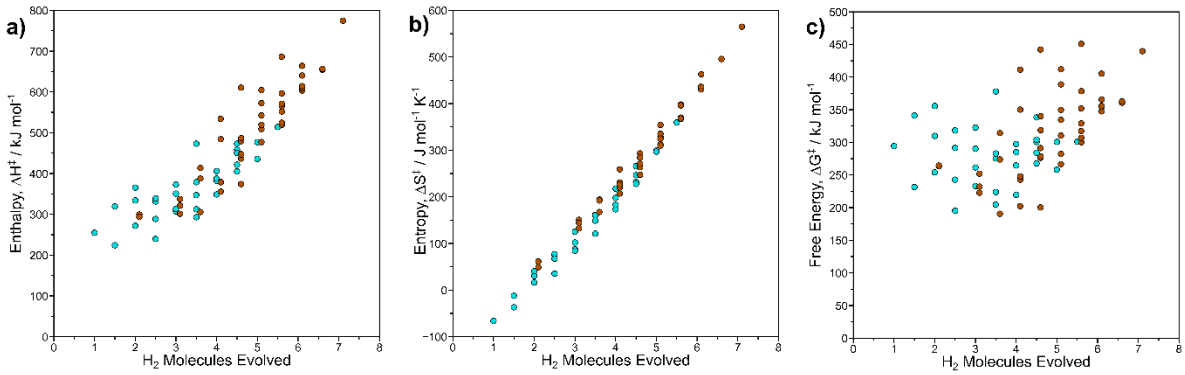

Figure S1. (a) Enthalpy (ΔH≠), (b) entropy (ΔS≠), and (c) free energy (ΔG≠) activation barriers for C–C bond cleavage of both extendable (light blue) and non-extendable (maroon) isobutane-derived intermediates on a H*-covered Ir(111) surface (593 K, 1 bar H_2).

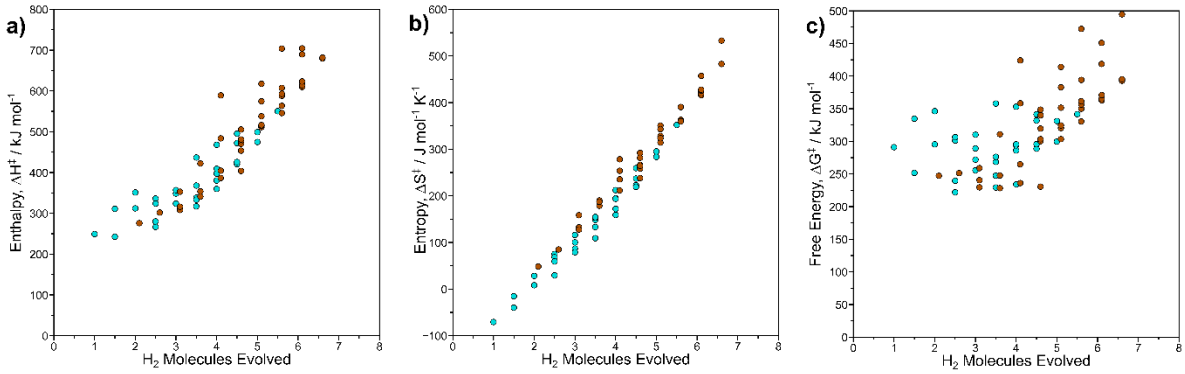

Figure S2. (a) Enthalpy (ΔH≠), (b) entropy (ΔS≠), and (c) free energy (ΔG≠) activation barriers for C–C bond cleavage of both extendable (light blue) and non-extendable (maroon) isobutane-derived intermediates on a H*-covered Pt(111) surface (593 K, 1 bar H_2).

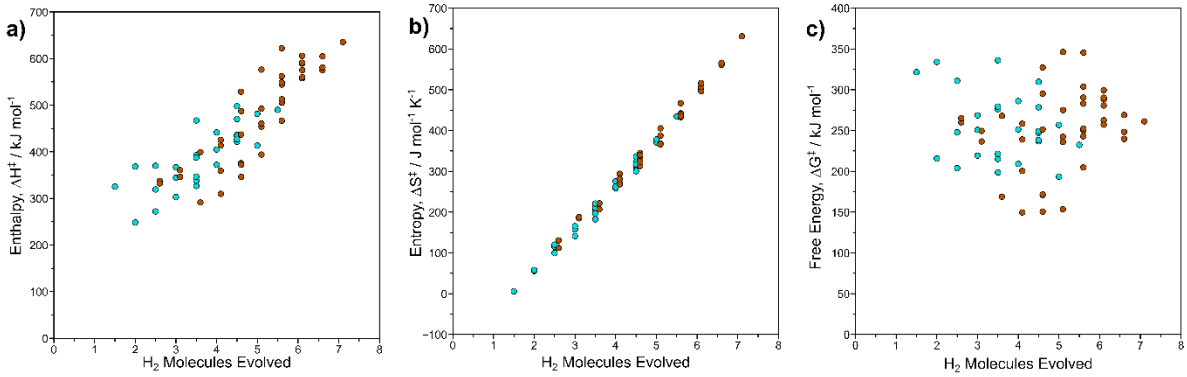

Figure S3. (a) Enthalpy (ΔH≠), (b) entropy (ΔS≠), and (c) free energy (ΔG≠) activation barriers for C–C bond cleavage of both extendable (light blue) and non-extendable (maroon) isobutane-derived intermediates on a H*-covered Ru(0001) surface (593 K, 1 bar H_2).

3. Influence of MASI on kinetic behavior

The dehydrogenated ethane intermediate concentration can be described with transition-state theory to associate the quasi-equilibrated reactant species with the formation of the transition state intermediate for three different cases: a bare surface, a H*-covered surface, and an ethylidyne (CH_3C^*)-covered surface shown below:

$$C_2H_6 + * \rightleftharpoons C_2H_2^{*\neq} + \lambda H_2 \qquad \lambda = 2 \qquad \text{(S10.1)}$$

$$C_2H_6 + 2H^* \rightleftharpoons C_2H_2^{*\neq} + \lambda H_2 \qquad \lambda = 3 \qquad \text{(S10.2)}$$

$$C_2H_3^* \rightleftharpoons C_2H_2^{*\neq} + \lambda H_2 \qquad \lambda = 0.5 \qquad \text{(S10.3)}$$

where λ represents the hydrogen pressure dependence of ethane hydrogenolysis with different mathematical definitions depending on the MASI species' hydrogen content.

The ethane hydrogenolysis turnover rate can be expressed as a function of the free energy to form the transition state ($\Delta G^{\neq}$).

$$\frac{r}{[L]} = \frac{k_B T}{h} exp\left(\frac{-\Delta G^{\neq}}{RT}\right) \frac{(C_2H_6)}{(H_2)^{\lambda}} \qquad \lambda = 2 \qquad \text{(S11.1)}$$

$$\frac{r}{[L]} = \frac{k_B T}{h} exp\left(\frac{-\Delta G^{\neq}}{RT}\right) \frac{(C_2H_6)}{(H_2)^{\lambda}} \qquad \lambda = 3 \qquad \text{(S11.2)}$$

$$\frac{r}{[L]} = \frac{k_B T}{h} exp\left(\frac{-\Delta G^{\neq}}{RT}\right) (H_2)^{-\lambda} \qquad \lambda = 0.5 \qquad \text{(S11.3)}$$

where each respective turnover rate is written with respect to the transition-state theory expressions above. Notably, the turnover rate's hydrogen pressure dependence varies with the MASI species, and under C_2^* MASI conditions (shown here as an ethylidyne species), pertinent for low H_2:alkane ratios with a hydrocarbon-covered surface, turnover rate is independent of alkane pressure.

4. H-desorption corrections*

The desorption corrections for a H*-covered surface are described in detail below.
The entropy of the H* adlayer is determined using thermodynamic formalisms:

$$S_{adlayer} = \frac{H_{adlayer} - G_{adlayer}}{T} \quad \text{(S12)}$$

To account for underpredictions of H* entropy, the entropy of the adlayer is adjusted by a factor (F in Eq. S13 below). For this work, a factor of 3.5 was used for all three metals.

$$S_{adj} = FS_{adlayer} \quad \text{(S13)}$$

The adjusted free energy of the adlayer is calculated using the adjusted entropy of the adlayer above.

$$G_{adj} = H_{adlayer} - TS_{adj} \quad \text{(S14)}$$

The desorption of H* from a H*-covered surface to form ℓ vacancies is depicted below:

$$16\mathrm{H}^* \rightleftharpoons (16-\ell)\mathrm{H}^* + \frac{\ell}{2}\mathrm{H}_2 \quad \text{(S15)}$$

Using the adjusted free energy of the adlayer, the free energy to form vacancies on the H*-covered metal surface (ΔG_{des}) can be determined using Eq. S15.

$$\Delta G_{des} = G_{adj} + \frac{\ell}{2}G_{H_2} - G_{adj,\ell=0} \quad \text{(S16)}$$

where G_{adj} is the adjusted free energy of the adlayer with ℓ vacancies from Eq. S15, G_{H_2} is the free energy of gaseous H_2, and $G_{adj,\ell=0}$ is the free energy of the H*-covered surface (1ML).

Table S1. Summary of Entropy Correction Factor (F) on Estimated Lambda Values at 593 K.

	$\lambda\ (F=3)$	$\lambda\ (F=3.5)$	$\lambda\ (F=4)$
Ir	3.15	3.08	3.03
Pt	2.99	2.88	2.77
Ru	4.25	4.25	4.25

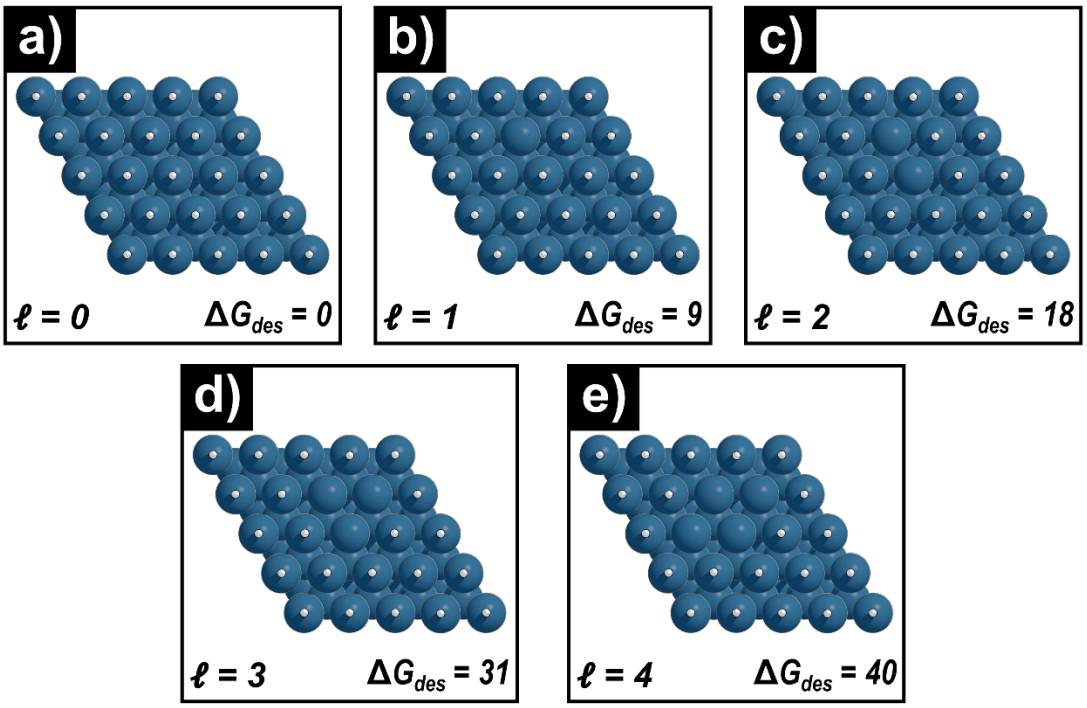

Figure S4. Structural images of the formation of 4 adjacent vacancies on a H*-covered Ir(111) surface. Desorption free energies are reported in kJ mol^{-1} and the number of vacancies (ℓ) is labeled for each structure.

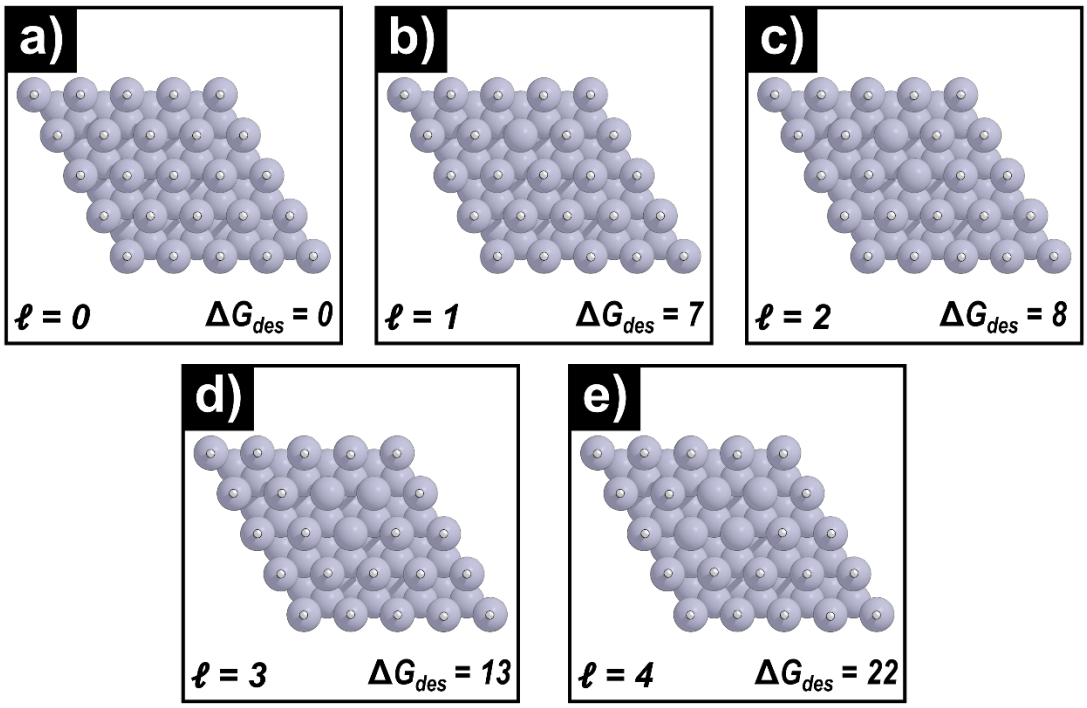

Figure S5. Structural images of the formation of 4 adjacent vacancies on a H*-covered Pt(111) surface. Desorption free energies are reported in kJ mol^{-1} and the number of vacancies (ℓ) is labeled for each structure.

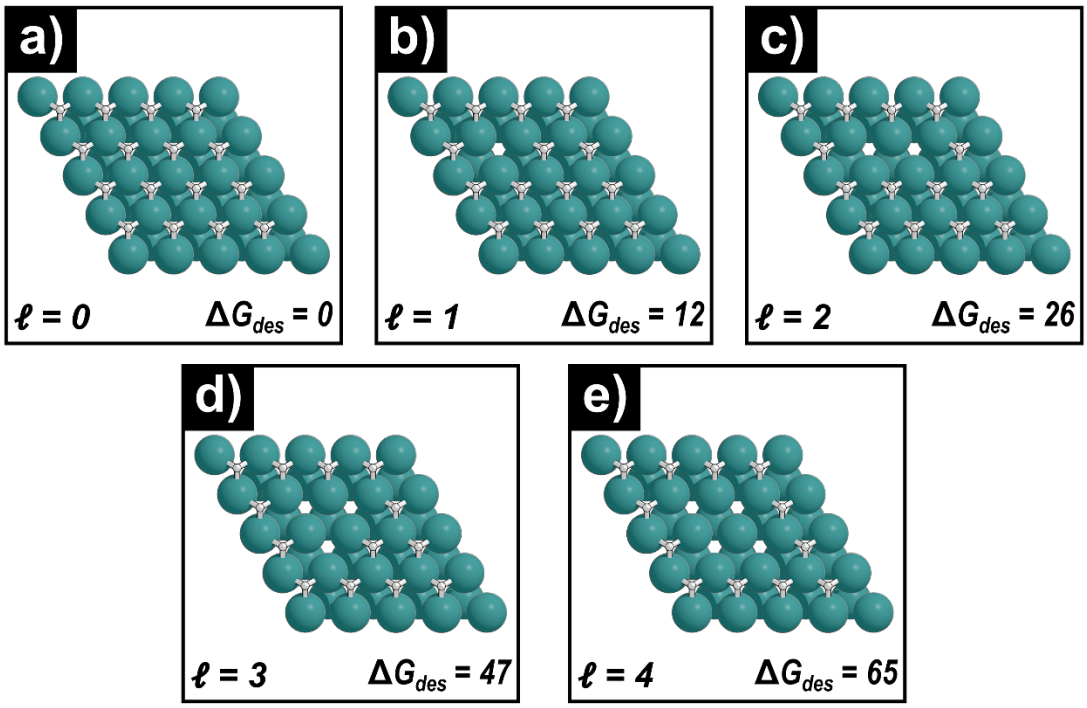

Figure S6. Structural images of the formation of 4 adjacent vacancies on a H*-covered Ru(0001) surface. Desorption free energies are reported in kJ mol^{-1} and the number of vacancies (ℓ) is labeled for each structure.

5. Isobutane Hydrogenolysis Structures

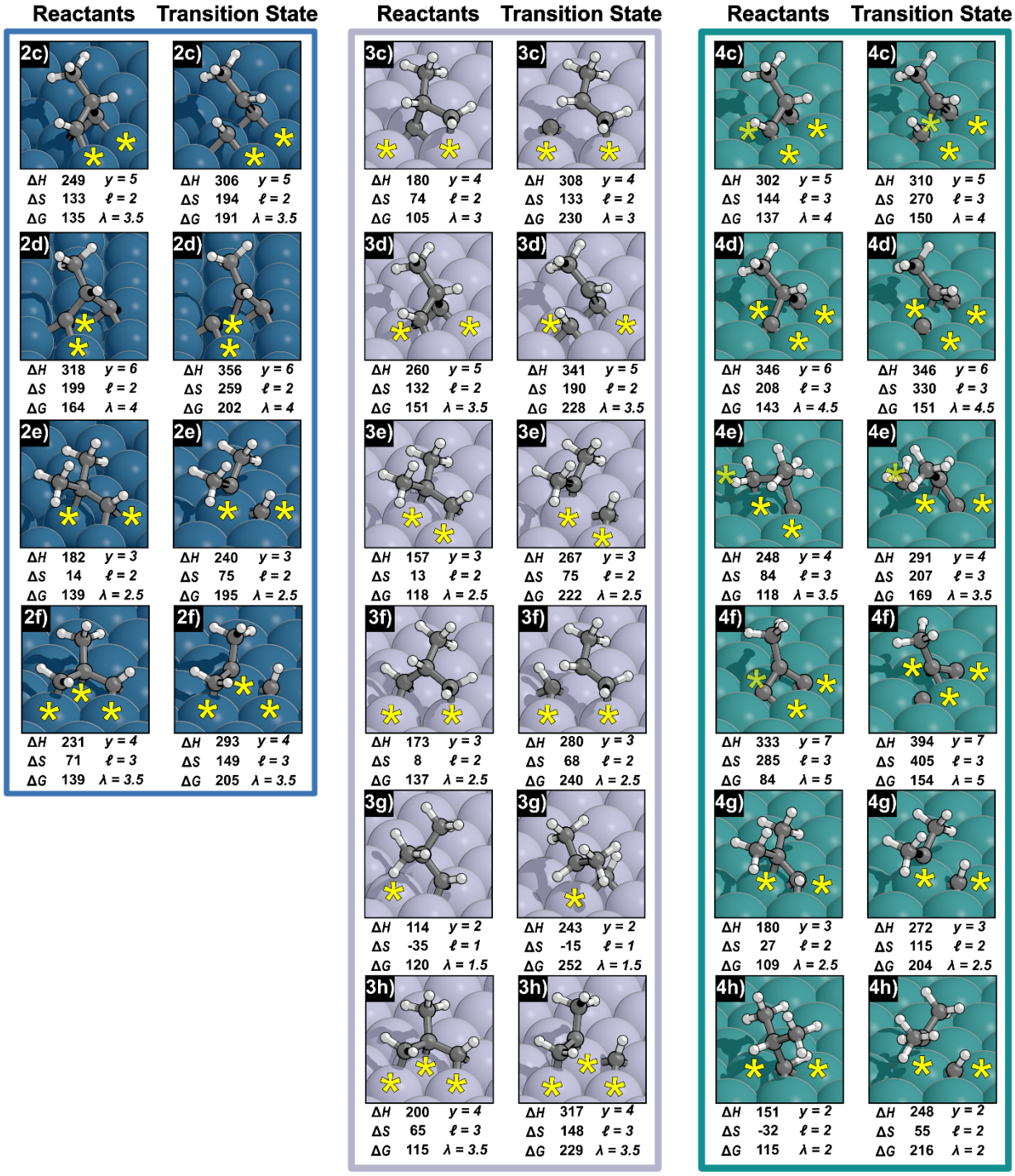

Figure S7. Reactant and transition state structures for isobutane hydrogenolysis on Ir (Fig. 2c-f), Pt (Fig. 3c-h), and Ru (Fig. 4c-h). Yellow asterisks mark potential configurations of vacancies (ℓ) around the isobutane-derived states. The enthalpy ΔH (kJ mol^{-1}), entropy ΔS (J mol^{-1} K^{-1}), and free energy ΔG (kJ mol^{-1}) values for the formation of each species are labeled below along with the H atoms removed (y), estimated site requirement of the transition state (ℓ), and the λ value associated with the mechanism on a H*-covered metal surface and the categorical extendibility of the mechanism.

6. Product Formation Energies

The details of the screening of transition states using product formation energies can be found below.

The product formation energy of any isobutane activation can be described as:

$$C_4H_{10} + 2^* \rightarrow C_3H_a{}^* + CH_b{}^* + \frac{y}{2}H_2 \quad \text{(S17)}$$

where $a + b = 10 - y$ or put more simply the total hydrogenation of the C_3 and C_1 fragments after activation is equal to the level of hydrogenation of the unsaturated isobutane-derived intermediate that undergoes C–C cleavage from Eq. 6 in the main text.
Using Eq. S17, the product formation free energy is calculated.

$$\Delta G_{prod} = G_{C_3H_a} + G_{CH_b} + \frac{y}{2}G_{H_2} - 2G_* - G_{C_4H_{10}} \quad \text{(S18)}$$

Thus, the product formation energy for any isobutane activation can be determined from the free energies of the C_1 and C_3 adsorbates formed from C–C cleavage.

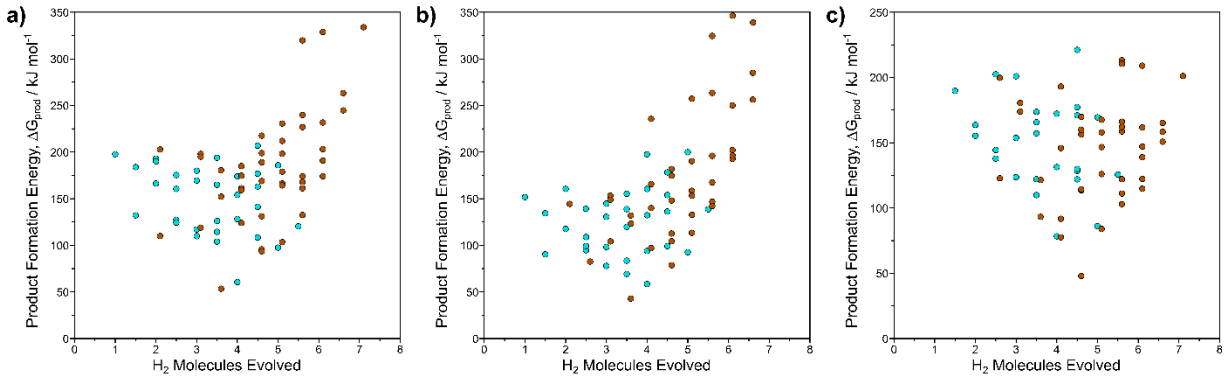

Figure S8. Product formation energies for isobutane activations on a H*-covered (a) Ir(111), (b) Pt(111), and (c) Ru(0001) surface as a function of H_2 molecules evolved. Product formation energies shown here include the desorption corrections for a H*-covered surface based on the number of unsaturated C atoms in the products.

Ultimately, the use of product formation free energies is to limit the scope of isobutane (or larger compound) activations explicitly modeled. Because DFT calculations can be computationally expensive, product formation energies can be used to weed out unlikely transition states from our search along the potential energy surface. However, product formation energies aren't as accurate as explicit free energy barrier determinations for DFT calculations (Fig. S8). Because of the inaccuracy of using product formation energies to predict transition state energies, many transition states are modeled based on the low product formation energy pathways.

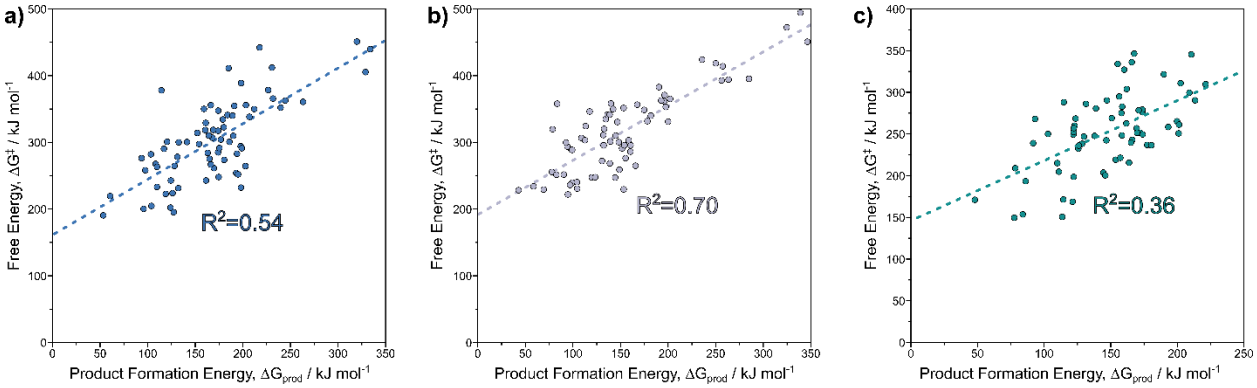

Figure S9. Parity plots comparing the free energy barrier of isobutane activations and the free energy to form the products on H*-covered (a) Ir(111), (b) Pt(111), and (c) Ru(0001) surfaces. Each subplot has a trendline showing the correlation along with the coefficient of determination for the linear trendline.

7. Partially Extendable Mechanisms

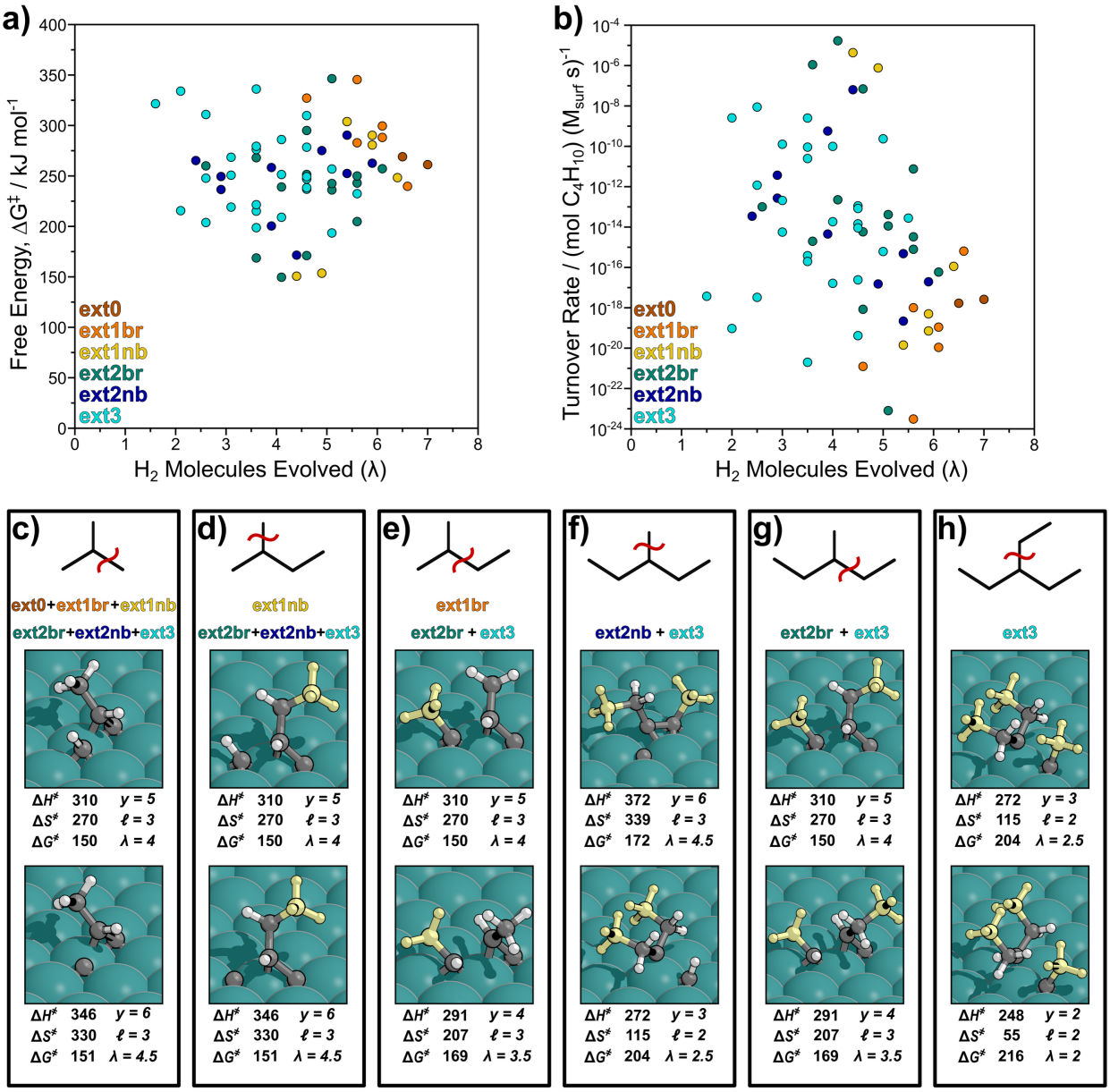

Figure S10. (a) Apparent free energy barriers ($\Delta G^{\neq}$), relative to a H*-covered surface, for C–C bond cleavage of isobutane-derived intermediates on an Ru(0001) surface (593 K, 1 bar H_2) split into 6 categories of extendibility. (b) Hydrogenolysis rates (593 K, 20 kPa isobutane, 10 bar H_2) derived from transition state theory (Eq. 8) for the same reactions. (c-h) Transition state structures of the two mechanisms with the highest hydrogenolysis rates for each model compound activation displayed above along with the associated mechanistic extendibilities. The yellow methyl groups are not actually present within the performed calculations, but represent how isobutane-derived transition states can serve as exemplars for the activation of larger molecules. The apparent enthalpy $\Delta H^{\neq}$ (kJ mol^{-1}), entropy $\Delta S^{\neq}$ (J mol^{-1} K^{-1}), and free energy $\Delta G^{\neq}$ (kJ mol^{-1}) barriers are labeled below along with the H atoms removed (y), estimated site requirement of the transition state (ℓ), and the degree of H_2 inhibition (λ) associated with the mechanism on a H*-covered metal surface.

Beyond the binary categorization of transition states as extendable or non-extendable, some transition states, such as the C–C activation shown in Fig. 4c, are partially extendable (i.e. not every terminal C atom is fully dehydrogenated). Considering these partially extendable mechanisms can allow us to make predictions, based on isobutane studies, of activations within molecules like 2-methylbutane and 3-methylpentane (along with 3-ethylpentane as done within the main text). More detailed extendibility "filters" are shown in Fig. S10a. Mechanisms classified as "ext0" cannot be extended, i.e., all three methyl groups in isobutane are fully dehydrogenated; those mechanisms can only be formed for isobutane reactions and cannot give insights into the activations of other larger alkanes. Ext1 mechanisms can be informative for 2-methyl-butane (2mb) activations as the chain can be extended in one direction, as such it can give insights into the activations of compounds like 2-methyl-butane, and larger 2-methyl-alkane species (species which have a tertiary C atom with two methyl groups). Here, whether the C_1 leaving group within the transition state can be extended or not (i.e., the C_1 leaving group is C*, and not CH_x*) is important, and noted here as "ext1br" if the C1 leaving group is extendable (which can give insights into the removal of ethyl groups from 2-methylbutane), and "ext1nb" if it is not (giving insights into the removal of methyl groups from 2-methylbutane). Similar distinctions exist for mechanisms extendable along two chains (ext2br and ext2nb), and fully extendable mechanisms are denoted as "ext3" here. Fig. S10 shows six example molecular activations and lists for each six which categories of extendibility are applicable to that specific activation. From those distinctions, we can filter the isobutane-based mechanisms considered here, to make predictions (from isobutane studies) of how branching would impact the regioselectivity of methyl- and ethyl-branched small alkanes on Ru catalysts, and these can be used to gain inferences into short (methyl) and longer branches in polyethylene and polypropylene polymers.

Methyl removal from 2-methylbutane (Fig. S10d) gives insights into removing methyl branches near the ends of polyolefin macromolecule backbones (but not methyl branches in the middle of those backbones) and resembles isobutane activation, as the mechanisms with the lowest apparent free energy barriers match those for isobutane (Fig. S10c). The two lowest $\Delta G^{\neq}$ values are for transition states with λ values of 4 and 4.5, respectively, suggesting that these activations would have similar H_2-pressure dependencies as those measured for isobutane activations on Ir.[2] For ethyl removal from 2-methylbutane (corresponding to backbone activation) near those same methyl branches, the lowest $\Delta G^{\neq}$ transition state matches that for isobutane activation, but the second-best isobutane activation cannot describe ethyl-removal from 2-methylbutane, and instead a mechanism that is less H_2-inhibited ($\lambda = 3.5$) is shown in Fig. S10. Comparing methyl removal (akin to loss of branching) and ethyl removal (akin to backbone activation), the most reactive transition state is the same for both, which would suggest that there is little regioselectivity for activations at the branch of 2-methylbutane.

As with 2-methylbutane activations, we can assess two distinct activations of 3-methylpentane: the methyl removal (akin to methyl-removals in polyethylene or polypropylene) and the ethyl removal (akin to backbone activation near a branch in polyethylene or polypropylene). DFT would predict, from these isobutane model calculations, that ethyl removal (Fig. S10g) from 3-

methylpentane would occur by the same mechanisms as ethyl removal from 2-methylbutane. In other words, activating a polyolefin backbone is predicted to occur with the same mechanism whether the methyl branch is in the middle or near the end of the polymer backbone. Methyl removal from 3-methylpentane, however, is predicted to occur through a different mechanism than methyl removal from 2-methylbutane. Removing methyls from 3-methylpentane (akin to methyl removal from the middle of polyolefin backbones) occurs with higher $\Delta G^{\neq}$ values (indicating lower rates) and higher λ values (indicating greater H_2 inhibition) than ethyl removals from 3-methylpentane (akin to backbone activations) or methyl removals from 2-methylbutane (akin to methyl removal from near the ends of polyolefin backbones). Given that most methyl branches in polypropylene are not near the ends of the macromolecule backbones, these data suggest that backbone activation would occur with higher rates than methyl removals from polypropylene. Furthermore, higher H_2 pressures would lead to greater preferences for backbone activation over methyl removal given that the λ values for ethyl-removal from 3-methylpentane is larger (4.5) than that for methyl removal from 3-methylpentane (4). These mechanistic preferences can be inserted into kinetic models for polyolefin upcycling to give greater insights into how the hydrocarbon melt evolves as the reaction progresses.

8. References

(1) McQuarrie, D. A. *Statistical Mechanics*; University Science Books: Sausalito, Calif, 2000.

(2) Flaherty, D. W.; Hibbitts, D. D.; Iglesia, E. Metal-Catalyzed C-C Bond Cleavage in Alkanes: Effects of Methyl Substitution on Transition-State Structures and Stability. *J. Am. Chem. Soc.* **2014**, *136* (27), 9664–9676. DOI: 10.1021/ja5037429.